35th Annual International Conference of the IEEE EMBS
Osaka, Japan, 3 - 7 July, 2013

Evaluation of an Image-based Tracking Workflow with Kalman Filtering for Automatic Image Plane Alignment in Interventional MRI

M. Neumann[1,3], L. Cuvillon[1], E. Breton[1], M. de Mathelin[1]

Abstract— **Recently, a workflow for magnetic resonance (MR) image plane alignment based on tracking in real-time MR images was introduced. The workflow is based on a tracking device composed of 2 resonant micro-coils and a passive marker, and allows for tracking of the passive marker in clinical real-time images and automatic (re-)initialization using the micro-coils. As the Kalman filter has proven its benefit as an estimator and predictor, it is well suited for use in tracking applications. In this paper, a Kalman filter is integrated in the previously developed workflow in order to predict position and orientation of the tracking device. Measurement noise covariances of the Kalman filter are dynamically changed in order to take into account that, according to the image plane orientation, only a subset of the 3D pose components is available. The improved tracking performance of the Kalman extended workflow could be quantified in simulation results. Also, a first experiment in the MRI scanner was performed but without quantitative results yet.**

I. INTRODUCTION

MINIMALLY invasive percutaneous procedures can be performed under MR-guidance. In order to monitor the real-time advancement of the needle during interventional MRI procedures, image planes are typically aligned on the instrument axis or to surrounding anatomical structures of interest. This real-time image plane orientation and positioning is currently performed manually, by a technologist at the MRI console, and its time efficiency strongly relies on his/her experience, as well as on his/her communication means with the physician standing inside the MRI room. As communication is rendered difficult by both the strong noise and visual occlusion of the MRI scanner, several systems have been presented for instrument detection and real-time scan plane control from inside the MRI room. These systems rely either on active or passive tracking devices.

Active tracking systems are either based on wired micro-coils measuring tracking gradients [1] or on optical tracking systems using cameras and markers [2] [3]. Main drawbacks of these approaches are dedicated tracking time and coil heating risk for the first type and need for an unobstructed line-of-sight between camera and marker for the second.

Passive approaches rely on image-based detection of passive tracking devices such as ferromagnetic objects [4], contrast agent filled stereotactic frames [5] or cylindrical markers [6] [7]. The limitations of these approaches are high susceptibility artifacts, the bulkiness of the tracking device and the use of dedicated tracking planes, respectively. Another technique is based on the use of resonant micro-coils that are tuned to the Larmor frequency of the scanner. In low flip angle acquisitions their signal is very well detectable, in contrast to the small signal of anatomical structures, so they can be used for tracking of surgical devices [8]. However, this is also their main disadvantage as their detection has to be performed in dedicated low flip angle images that cannot be used for image-guided procedures.

Main advantages of image-based tracking techniques are that they need neither expensive instrumentation nor any calibration, as markers and patients are depicted in the same images. Nevertheless, the quality of tracking in images depends on spatial resolution and robustness of detection algorithms. The use of the Kalman filter has been proposed to increase the tracking robustness of interventional devices in image-guided interventions. In [9], the benefits of introducing the Kalman filter in the tracking of an MRI compatible robot have been demonstrated. In the field of ultrasound guided percutaneous interventions, the Kalman filter has been proposed for position prediction of a manually inserted needle and has proven to stabilize the tracking results [10].

In [11], we presented a workflow using resonant micro-coils for the initialization of the detection and a passive marker for real-time automatic scan plane alignment. Main advantages of that approach are 1) automatic detection initialization, 2) reduced dedicated acquisition time (only one acquisition for initialization) and 3) the 3D depiction of the anatomy through 2 orthogonal image planes. The current paper aims to improve the proposed tracking by taking advantage of the predictive and noise filtering characteristics of a Kalman filter to estimate the passive marker position and orientation. Simulations have been carried out in order to evaluate the performance of the Kalman filter. Tracking experiments were also performed using that approach.

II. MATERIALS

A. Tracking device

As described in [11], the tracking device (Fig. 1c) is composed of 2 resonant micro-coils (Fig. 1a) rigidly fixed at the endings of a passive marker (Fig. 1b). Micro-coils, wound around small plastic tubes, are tuned to the Larmor frequency of the 1.5 T MRI scanner and contain a contrast agent / water solution (Gd-DTPA 5 mM) as signal source. The passive marker is a cylinder (length: 9 cm, diameter: 3.5 cm) filled with the same contrast agent dilution.

Manuscript received February 4, 2013.

[1]ICube, Université de Strasbourg, CNRS; Strasbourg, France.

[3]Correspondence to: Markus Neumann, ICube IRCAD, 1 Place de l'Hôpital, 67091 Strasbourg (France); email: m.neumann@unistra.fr

B. MRI scanner and scanner settings

All experiments were performed using the body coil in an open bore 1.5 T MRI scanner (MAGNETOM Aera, Siemens AG, Erlangen, Germany). An interactive, real-time, multi-slice TrueFISP sequence (Beat_IRTTT [12], Siemens Corporate Research & Technology, USA) was used for image acquisition. The passive marker is used for detection in clinical real-time images. Imaging parameters of the clinical real-time sequence include: matrix 202×224, FOV 450×450 mm^2, slice thickness 4 mm, TE 2.2 ms, TR 4.1 ms, flip angle 50°, bandwidth 260 Hz/Px. The 2 micro-coils are used for detection in dedicated low flip angle acquisitions with the same imaging parameters except: slice thickness 100 mm and flip angle 1°. Note that these projection images are not clinically usable by the physician. Image acquisition time is 819 ms but the image update time is lengthened to 1.2 s to allow for data transfer (image and scan plane control) and image processing.

III. Methods

A. Workflow

The principle of the workflow, previously described in [11], is to control 2 orthogonal scan planes (simple oblique sagittal and double oblique transversal) and to align them automatically along the main axis of the tracking device. The workflow described hereafter is the same, with the only difference that both orthogonal scan planes are simple oblique.

1) Initialization: A dedicated low flip angle transversal projection at the MRI scanner isocenter is acquired. The micro-coils are detected, the 3D pose (position and orientation) of a simple oblique sagittal plane aligned on the main axis of the tracking device is calculated and sent to the MRI scanner.

2) Image Plane alignment: The first real-time simple oblique sagittal image (I_1) is acquired at the pose calculated during initialization. The passive marker is then detected in this image, its 3D pose (P_1) is computed and the corresponding pose of a new simple oblique transversal image (I_2) aligned with the marker is calculated. After

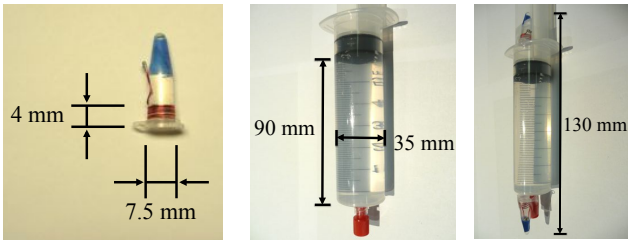

(a) (b) (c)

Fig. 1: (a) Micro-coil wound around a plastic tube filled with contrast agent solution. (b) Passive marker consisting of a syringe filled with the same contrast agent solution. (c) Assembled test device with 2 micro-coils at endings of the passive marker.

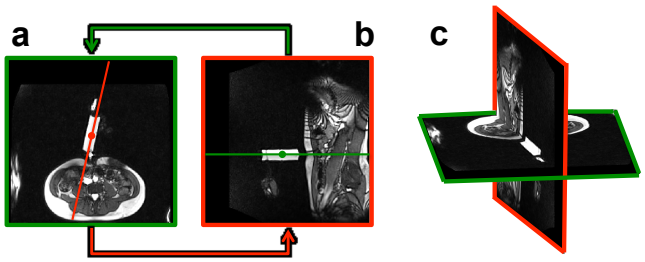

Fig. 2: Principle of Workflow: 2 orthogonal image planes, transversal (a) and sagittal (b), update their positions and orientations mutually, according to the detected passive marker. A 3D view is presented in (c).

acquisition of I_2, the current pose (P_2) of the passive marker is again detected in the image in order to update position and orientation of a new sagittal image (I_3). From then on, the 2 orthogonal image planes (sagittal/transversal) alternate and update their positions and orientations mutually according to the detected pose of the passive marker (Fig. 2). In case of a detection failure of the passive marker, the workflow will be reinitialized.

In the described workflow, it is assumed that the 3D pose of the tracking device stays nearly constant between 2 images. This means that after acquisition of the current image (I_k) and detection of the 3D pose (P_k) of the tracking device, the following image plane (I_{k+1}) will be aligned to P_k. The 3D pose of the marker is here defined by $P_k = (x, y, z, \alpha, \beta)^T$ with $(x, y, z)^T$ the position of the marker and $(\alpha, \beta)^T$ the orientation angles of the marker main axis. Angle α allows to rotate a pure sagittal plane (y-0-z) to the marker-aligned simple oblique sagittal plane (rotation around z-axis of the MRI scanner). Angle β is the corresponding angle between a pure transversal plane (x-0-y) and the marker-aligned simple oblique transversal plane (rotation around x-axis).

However, changes of position normal to the current image plane (I_k) and the pose component defining the orientation of I_k (α or β) cannot be detected. In this context, only a partial update of the detected 3D pose between 2 consecutive image planes is possible.

In order to improve the alignment of the following image plane (I_{k+1}), the current alignment algorithm is extended by a Kalman filter that predicts the next 3D pose (P_{k+1}) of the tracking device by considering its past values.

B. Kalman filtering

The Kalman filter predicts the future pose of the tracking device based on previous detections, in order to orient and position the following image plane. The process state is represented by the pose and its derivative:

$$X_k = \begin{pmatrix} P_k \\ \dot{P}_k \end{pmatrix} \tag{1}$$

The process model is given by the linear equation

$$X_k = AX_{k-1} + n_{k-1}, \tag{2}$$

with a measurement Z_k which is

$$Z_k = HX_k + m_k, \tag{3}$$

where n_k and m_k represent process noise and measurement noise, respectively. Their gaussian probability distributions are

$$p(m_k) \sim N(0, R) \tag{4}$$
$$p(n_k) \sim N(0, Q), \tag{5}$$

where R and Q represent the measurement noise covariance and the process noise covariance, respectively. As constant velocity is assumed for the marker motion, the transition matrix can be written as

$$A = \begin{bmatrix} I_{5\times5} & \delta t \cdot I_{5\times5} \\ 0 & I_{5\times5} \end{bmatrix}, \tag{6}$$

where δt is the time step between 2 image acquisitions and $I_{5\times5}$ is a 5×5 identity matrix. As the whole pose of the marker is assumed to be detected directly in the images, the observation matrix is given by

$$H = \begin{bmatrix} I_{5\times5} & 0 \end{bmatrix}. \tag{7}$$

The filter has to be updated with the 3D pose of the marker at each image acquisition. However, as described in section III-A.2, only a subset of the 3D pose is available on each acquired image. When a component is totally unavailable (normal to a pure sagittal or transversal image plane), its value from the previously acquired image is kept, as the Kalman filter expects a full measurement vector. Therefore, the predictive performance of the Kalman filter decreases, if all measured components are taken into account with the same weight. This effect could be compensated by adapting dynamically the measurement noise covariance matrix R in order to weight the confidence of a measured pose component as a function of the current image plane orientation. Thus, the measurement noise covariance values for position components normal to the image plane vary on an interval $[10^{-5};1]$ and are a function of α and β for sagittal and transversal image planes, respectively. As an orientation component can either be detected or not on an image plane, its measurement noise covariance is not gradually adapted but set to the interval boundaries in a binary manner. Thus, R is obtained as

$$R = \begin{bmatrix} 10^{-a} & 0 & 0 & 0 & 0 \\ 0 & 10^{-b} & 0 & 0 & 0 \\ 0 & 0 & 10^{-c} & 0 & 0 \\ 0 & 0 & 0 & 10^{-d} & 0 \\ 0 & 0 & 0 & 0 & 10^{-e} \end{bmatrix} \tag{8}$$

with $a = 5$, $b = 5cos(\beta)$, $c = 5\,|sin(\beta)|$, $d = 5$, $e = 0$ for transversal image planes and $a = 5\,|sin(\alpha)|$, $b = 5cos(\alpha)$, $c = 5$, $d = 0$, $e = 5$ for sagittal image planes.

C. System Architecture

An ethernet connection between an external PC and the MRI console PC is established. A custom program allows for communication between the PCs via a proprietary Siemens protocol (ReModProt, Siemens Corporate Research & Technology, USA) and implementation of the presented workflow including image reception on the external PC, image processing, command calculation and sending of the command to the MRI console PC.

D. Simulations and feasibility experiments

Performance of the Kalman prediction has been evaluated through simulations and a feasibility experiment. Therefore, a program has been implemented that simulates the motion of the tracking device in space and the function of the MRI console PC, by creating and sending simulated images to the program implementing the presented workflow with and without the Kalman filter. This program performs marker detection in the received image, calculates the next orthogonal scan plane accordingly and sends the corresponding command to the simulator, which returns the image corresponding to the requested scan plane. A feasibility experiment was performed in the MRI scanner, where an operator moved the tracking device on random trajectories inside the MRI bore.

IV. Results

A trajectory of the tracking device was simulated (translational velocity: 9 mm/s, rotational velocity: 2°/s) and the predictive performance of the Kalman filter was evaluated by comparing the detected 3D poses of the initial workflow and of the Kalman extended workflow. Fig. 3 represents the real trajectory and the detected ones for every component of the 3D pose as well as the corresponding root-mean-square errors (RMSE). As expected, the Kalman filter improves the device tracking during continuous movements, as its algorithm considers past pose measurements and a constant velocity model. However, the initial workflow does not apply any process model and as some components of the 3D pose are not available on every acquired image, their previous values are kept. As a consequence, one can observe a "step-pattern" deviating from the real trajectory for those components. The benefit of the Kalman filter is observable as it adjusts this "step-pattern" for x, z, α, β pose components. The y component is well detectable on all image planes due to the small image plane orientations α and β and thus the difference of the detection between the initial workflow and the Kalman extended workflow is less obvious. An experiment was carried out in the MRI scanner, but could not be quantified yet.

V. CONCLUSIONS

In this work a fully automatic scan plan alignment workflow for interventional MRI has been extended by a Kalman filter with dynamically adapted measurement noise covariances. First simulation results have shown that tracking performance is improved. Currently, a translation test bench is being developed for use inside the MRI scanner in order

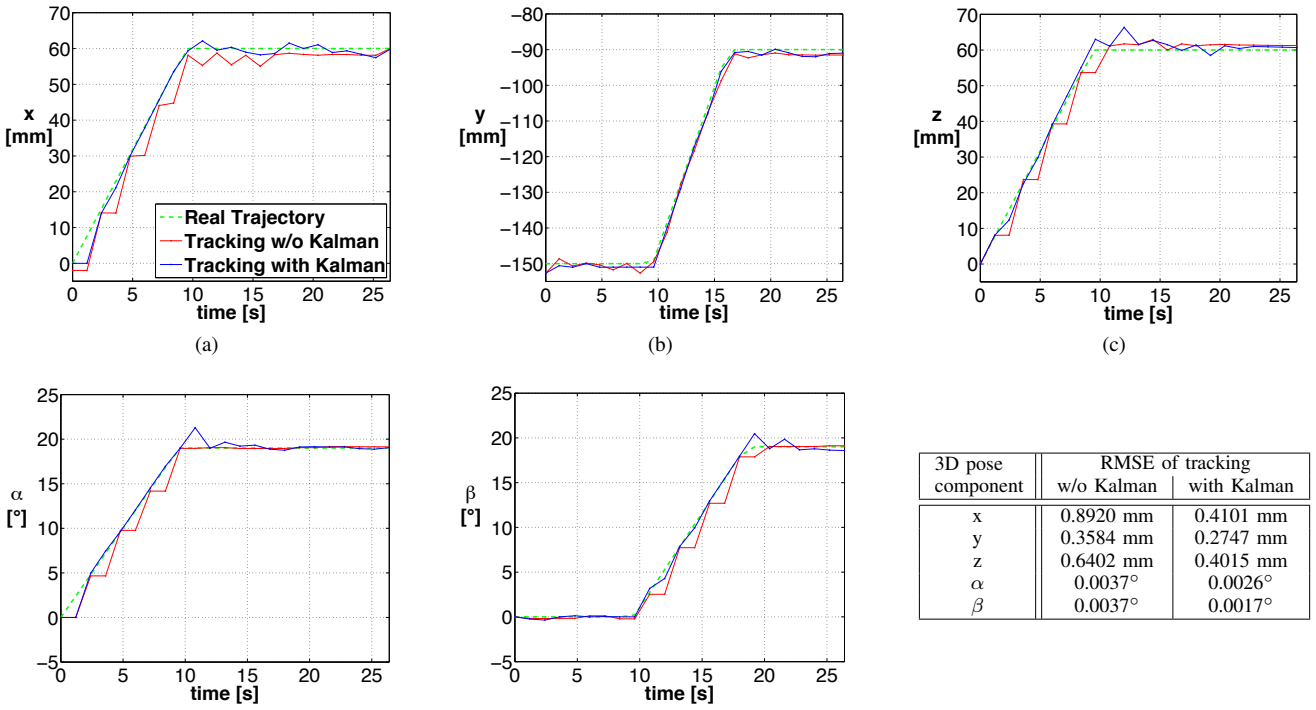

(f)

3D pose component	RMSE of tracking w/o Kalman	RMSE of tracking with Kalman
x	0.8920 mm	0.4101 mm
y	0.3584 mm	0.2747 mm
z	0.6402 mm	0.4015 mm
α	0.0037°	0.0026°
β	0.0037°	0.0017°

Fig. 3: Simulation results of passive marker tracking for the initial workflow and for the Kalman extended workflow are represented for every component of the 3D pose (a-e), as well as the corresponding root-mean-square errors (f).

to move the marker along a given trajectory to make experimental evaluation possible.

ACKNOWLEDGMENT

Authors would like to thank Pr. Afshin Gangi and his team for their support.

REFERENCES

[1] K. Qing, L. Pan, B. Fetics, F. K. Wacker, S. Valdeig, M. Philip, A. Roth, E. Nevo, D. L. Kraitchman, A. J. v. d. Kouwe, and C. H. Lorenz, "A multi-slice interactive real-time sequence integrated with the EndoScout tracking system for interventional MR guidance," in *Proceedings of the 18th Annual Meeting of ISMRM*, 2010, p. 1860.

[2] R. Blanco Sequeiros, R. Klemola, R. Ojala, L. Jyrkinen, E. Lappi-Blanco, Y. Soini, and O. Tervonen, "MRI-guided trephine biopsy and fine-needle aspiration in the diagnosis of bone lesions in low-field (0.23 t) MRI system using optical instrument tracking." *European Radiology*, vol. 12, no. 4, pp. 830–835, Apr. 2002.

[3] R. Viard, N. Betrouni, J. Rousseau, S. Mordon, O. Ernst, and S. Maouche, "Needle positioning in interventional MRI procedure: real time optical localisation and accordance with the roadmap," in *Engineering in Medicine and Biology Society, 2007. EMBS 2007. 29th Annual International Conference of the IEEE*, 2007, pp. 2748–2751.

[4] O. Felfoul, J. B. Mathieu, G. Beaudoin, and S. Martel, "In vivo MR-tracking based on magnetic signature selective excitation," *IEEE Transactions on Medical Imaging*, vol. 27, no. 1, pp. 28–35, Jan. 2008, PMID: 18270059. [Online]. Available: http://www.ncbi.nlm.nih.gov/pubmed/18270059

[5] S. P. DiMaio, E. Samset, G. Fischer, I. Iordachita, G. Fichtinger, F. Jolesz, and C. M. Tempany, "Dynamic MRI scan plane control for passive tracking of instruments and devices," in *Proceedings of the 10th international conference on Medical image computing and computer-assisted intervention*, ser. MICCAI'07. Berlin, Heidelberg: Springer-Verlag, 2007, pp. 50–58. [Online]. Available: http://portal.acm.org/citation.cfm?id=1775835.1775843

[6] F. Maier, A. Krafft, R. Stafford, J. Yung, R. Dillmann, W. Semmler, and M. Bock, "3D passive marker tracking for MR-Guided interventions," in *Proceedings of the 19th Annual Meeting of ISMRM*, 2011, p. 3749.

[7] F. Maier, A. Krafft, R. de Oliveira, W. Semmler, and M. Bock, "MRPen 3D marker tracking for percutaneous interventions," in *Proceedings of the 17th Annual Meeting of ISMRM*, 2009, p. 4421.

[8] M. Rea, D. McRobbie, H. Elhawary, Z. Tse, M. Lamperth, and I. Young, "Sub-pixel localisation of passive micro-coil fiducial markers in interventional MRI," *Magnetic Resonance Materials in Physics, Biology and Medicine*, vol. 22, pp. 71–76, 2009, 10.1007/s10334-008-0143-1. [Online]. Available: http://dx.doi.org/10.1007/s10334-008-0143-1

[9] C. Bergeles, L. Qin, P. Vartholomeos, and P. Dupont, "Tracking and position control of an MRI-Powered needle-insertion robot," in *2012 Annual International Conference of the IEEE Engineering in Medicine and Biology Society (EMBC)*, San Diego, CA, Sep. 2012.

[10] Y. Zhao, H. Liebgott, and C. Cachard, "Tracking micro tool in a dynamic 3D ultrasound situation using kalman filter and RANSAC algorithm," in *2012 9th IEEE International Symposium on Biomedical Imaging (ISBI)*, May 2012, pp. 1076 –1079.

[11] M. Neumann, E. Breton, L. Cuvillon, L. Pan, C. Lorenz, and M. de Mathelin, "Evaluation of an image-based tracking workflow using a passive marker and resonant micro-coil fiducials for automatic image plane alignment in interventional MRI," in *2012 Annual International Conference of the IEEE Engineering in Medicine and Biology Society (EMBC)*, Sep. 2012, pp. 1085 –1088.

[12] L. Pan, J. Barbot, S. Shea, S. Patil, K. Kirchberg, G. Meredith, T. Meng, E. Kholmovski, S. Vijayakumar, K. Vij, M. Guttmann, P. Piferi, K. Jenkins, and C. Lorenz, "An integrated system for catheter tracking and visualization in MR-Guided cardiovascular interventions," in *Proceedings of the 19th Annual Meeting of ISMRM*, 2011, p. 195.